A Possible Role for the Covalent Heme−Protein Linkage in Cytochrome *c* Revealed via Comparison of *N*-Acetylmicroperoxidase-8 and a Synthetic, Monohistidine-Coordinated Heme Peptide†

Aaron B. Cowley,‡ Gudrun S. Lukat-Rodgers,§ Kenton R. Rodgers,§ and David R. Benson*,‡

Department of Chemistry, University of Kansas, Lawrence, Kansas 66045, and Department of Chemistry, North Dakota State University, Fargo, North Dakota 58105

Received August 26, 2003; Revised Manuscript Received October 25, 2003

ABSTRACT: *N*-Acetylmicroperoxidase-8 (**1**) contains heme and residues 14−21 of horse mitochondrial cytochrome *c* (cyt *c*). The two thioether bonds linking protein to heme in cyt *c* are present in **1**, and the native axial ligand His-18 remains coordinated to iron. As an approach to probing structural or functional roles played by the double covalent heme−protein linkage in cyt *c*, we have initiated a study in which the properties of **1** are compared with those of a synthetic mono-His coordinated heme peptide containing a single covalent linkage (**2**). One consequence of the greater conformational restriction imposed on peptide conformation in **1** is that His−Fe(III) coordination is ∼1.4 kcal/mol more favorable in **1** than in **2**. This highlights a clear advantage conferred to cyt *c* by having two covalent heme−protein linkages rather than one: greater thermodynamic stability of the protein fold. EPR (11 K) and resonance Raman (298 K) studies reveal that **1** and **2** exhibit a thermal high-spin/low-spin ferric equilibrium but that low-spin character is considerably more pronounced in **1**. In addition, the thioether 2-(methylthio)ethanol (MTE) coordinates 0.5 kcal/mol more strongly to **1** than to **2** in 60:40 H_2O/CH_3OH and only triggers the expected conversion of iron to the low-spin state characteristic of ferric cyt *c* in the case of **1**. This demonstrates that the axial ligand field provided by an imidazole and a thioether is too weak to induce a high-spin to low-spin conversion in a ferric porphyrin. Our results suggest that a conformationally constrained double covalent heme−protein linkage, as exists in **1** and its parent protein cyt *c*, is an effective solution that nature has evolved to circumvent this limitation. We propose that the stronger His−Fe(III) coordination enabled by such a linkage serves to markedly enhance the effective ligand field strength of His-18. Our studies with **1** and **2** suggest that a double covalent linkage in cyt *c* may also enable energetically more favorable trans ligation of Met-80 than would be possible if only a single linkage were present. This would serve to further increase the stability of the protein fold and perhaps to increase the effective ligand field strength of Met-80 as well.

One of the distinguishing characteristics of mitochondrial cytochrome *c* (cyt[1] *c*) is covalent attachment of protein to heme via thioether linkages to the side chains of two cysteine residues, which comprise part of a conserved Cys(14)-X-X-Cys(17)-His(18) motif (*1*). The imidazolyl side chain of His-18 serves as an axial ligand to heme, with the second axial ligand provided by the thioether side chain of Met-80. The ligand field provided by His-18 and Met-80 in cyt *c* is sufficiently strong to favor a low-spin state for iron in both the ferrous and ferric oxidation states. The bond between Met-80 and iron is markedly weaker in the ferric protein than in the ferrous protein, however (*2*).

Cyt *c* unfolds completely upon removal of heme (*3*, *4*), demonstrating the importance of heme−protein interactions to protein conformational stability. Reconstituting the apoprotein with ferric heme yields a poorly organized noncovalent complex, which does not exhibit His−Met coordination (*5*, *6*). Mutation of Cys-14 to Ala in yeast cyt *c* yields a protein in which His-18 and Met-80 are maintained as heme axial ligands (*7*) but which exhibits greater conformational flexibility than the wild-type protein. It can therefore be concluded (1) that one covalent linkage between protein and heme is sufficient to induce the protein fold, (2) that two linkages offer greater stabilization of the folded protein than does one, and (3) that coordination of Met-80 to Fe(III) in cyt *c* requires the preorganization offered by an already folded protein. Two points of covalent attachment between heme and protein in cyt *c* would be expected to limit the conformational freedom of residues 14−17, which should diminish the entropy difference between the native and unfolded states. This factor has been suggested to favor the native state of mitochondrial cyt *c* by as much as 2 kcal/mol (*8*).

† This work was supported by a grant to D.R.B. from the American Heart Association, Heartland Affiliate (0151412Z), and by grants to K.R.R. from the USDA (2001-35318-11204) and the Hermann Frasch Foundation (446-HF97).

* Correspondence should be addressed to this author. Telephone: (785) 864-4090. Telefax: (785) 864-5396. E-mail: drb@ku.edu.

‡ University of Kansas.

§ North Dakota State University.

[1] Abbreviations: cyt, cytochrome; CD, circular dichroism; RR, resonance Raman; EPR, electron paramagnetic resonance; NMR, nuclear magnetic resonance; MTE, 2-(methylthio)ethanol.

10.1021/bi035531p CCC: $27.50
Published on Web 01/21/2004

Chart 1

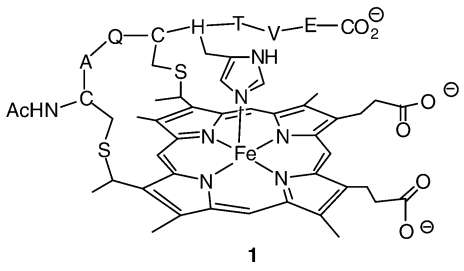

1

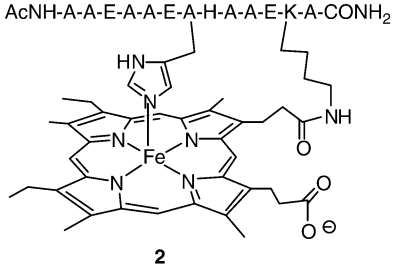

2

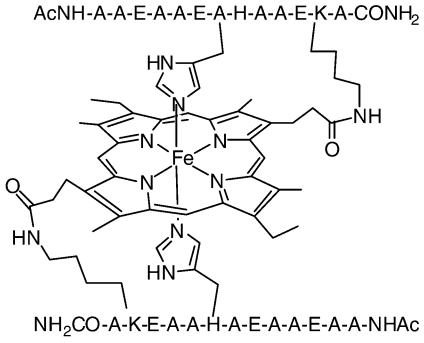

3

Treatment of horse heart cyt *c* with pepsin and trypsin (*9*), followed by N-terminal acetylation (*10*−*13*) yields *N*-acetylmicroperoxidase-8 (**1**; Chart 1), so-called because it catalyzes peroxidase reactions (*14*). The peptide in **1** corresponds to residues 14−21 of cyt *c*. His-18 is maintained as an axial ligand in **1** (*15*), and resonance Raman (RR) studies indicate that iron is hexacoordinated with water likely occupying the second axial coordination site (*11*, *16*, *17*). NMR studies have shown that the secondary structure exhibited by residues 14−18 in cyt *c*, which includes a single turn of 3_{10} helix spanning residues 14−17 (*18*, *19*), is retained in **1** (*20*). RR (*16*) and computational studies (*21*−*23*) further indicate that the pronounced ruffling of heme in cyt *c* (*19*) is retained in **1**. Inducing heme ruffling, a feature that is conserved across species and is of potential functional importance (*24*, *25*), thus represents a role played by the covalent heme−protein linkage in cyt *c*.

The aquo ligand in **1** and related cyt *c* heme peptides can be displaced by exogenous ligands (*26*). For example, the low-spin His−Met coordination sphere of ferric cyt *c* can be reproduced in the presence of a large concentration of a thioether in aqueous solution (*10*, *17*, *27*). Such complexes cannot be prepared from a simple iron porphyrin, an imidazole, and a thioether because bisimidazole coordination is strongly favored.

To further address potential structural and functional roles of the double covalent heme−protein linkage in cyt *c*, it might be instructive to compare the properties of **1** with those of a heme peptide containing a single linkage. Although a variety of synthetic, monoimidazole-coordinated iron porphyrins have appeared in the literature (*28*−*34*), only one has been reported to form a low-spin thioether complex in the ferric oxidation state, successfully reproducing the coordination sphere and spin state of ferric cyt *c* (*30*). Model compounds with a single intramolecular thioether, or with one thioether and one imidazole, have also failed to produce a ferric cyt *c* model (*32*, *35*−*40*). It has been proposed (*28*, *30*) that failures in many attempts resulted because the studies (including the reportedly successful one) (*30*) were performed in organic solvents of low polarity. Under those conditions, anions such as the counterion to Fe(III) that is invariably present coordinate preferentially to iron in order to achieve charge neutrality. Mono-His-coordinated heme peptide **2** allows us to circumvent this problem because it is soluble in water and other highly polar solvents (*33*). The 13-residue helical peptide in **2** is attached to iron mesoporphyrin IX via a single covalent linkage, an amide bond between a mesoheme propionate group and the ϵ-amino nitrogen of lysine-12 (Lys-12).

All of the porphyrin substituents in **1** and **2** are saturated and occupy the same relative positions around the ring. Furthermore, each compound will bear four negative charges at neutral pH (two heme propionates and the α- and γ-carboxylates of Glu-21 in **1**; one heme propionate and three Glu γ-carboxylates in **2**), with the only positive charge in each case arising from Fe(III). A side-by-side comparison of the properties of **1** and **2** therefore has the potential to provide insight into structural and functional roles played by the double heme−peptide covalent linkage in the former. In this report, we present the results of a study in which the spectroscopic properties of ferric **1** and **2** are compared, as well as their interactions with several exogenous ligands.

EXPERIMENTAL PROCEDURES

Materials. All reagents were of commercial grade and were used without further purification. Preparation of **1** (*13*) and **2** (*33*) was accomplished by previously reported methods. It should be noted that **2** exists in two isomeric forms, with the peptide attached to either the 6- or 7-propionate group of the heme. Although it has not proven possible to separate these isomers, it is not expected that the different points of attachment will exert a significant effect on heme properties.

Electronic Absorption Spectroscopy. Electronic absorption spectra were recorded on Kontron Uvikon 9410 and Varian Cary 100 Bio UV/visible spectrophotometers. The temperature in the former is controlled by a circulating water bath and monitored with an Omega Model HH200 thermometer with T thermocouple (±0.2 °C). The latter contains a Peltier-thermostated cell holder and a dedicated temperature probe accessory (±0.1 °C). A quartz cuvette with 1.0 cm path length was used in all cases. Ligand binding titrations were performed in 60:40 (v/v) H_2O/CH_3OH buffered to pH 8.0 with 50 mM potassium phosphate, except in the case of MTE where the solutions were unbuffered. The concentration of **1** or **2** was held constant at 3−5 μM while that of the ligand was varied. Data were fit (Igor Pro, v.4.0; Wavemetrics, Inc.) to a standard equation describing a 1:1 binding isotherm (eq 1), where A_λ is the absorbance at a given wavelength, $A_{\lambda(\mathrm{HP})}$

$$A_\lambda = A_\lambda(\mathrm{HP}) - \left[\left(\frac{[\mathrm{HP}][\mathrm{L}]}{K_\mathrm{d}}\right)\Big/\left(1 + \frac{[\mathrm{L}]}{K_\mathrm{d}}\right)\right](\epsilon_{\lambda(\mathrm{HP})} - \epsilon_{\lambda(\mathrm{L-HP})}) \quad (1)$$

is the corresponding absorbance for heme peptide (HP) **1** or

2 in the absence of ligand, $\epsilon_{\lambda(HP)}$ and $\epsilon_{\lambda(L-HP)}$ are the extinction coefficients at that wavelength in the absence of ligand and in the presence of a saturating concentration of the ligand, respectively, [L] is the concentration of free ligand, and K_d is the dissociation constant. The value of $\epsilon_{\lambda(L-HP)}$ was allowed to vary to obtain the best fit.

Electron Paramagnetic Resonance Spectroscopy. X-band EPR spectra were recorded on a Bruker EMX EPR spectrometer equipped with an ER4102ST cavity. An Oxford temperature controller ITC503 with liquid He was used to control the sample temperature. Samples (11 μM) were dissolved in 3:1:1 H_2O/CH_3OH/glycerol solution buffered to pH 8.0 with 100 mM sodium phosphate. Instrumental parameters: microwave power, 2.0 mW at 9.5 GHz; modulation, 10 G at 100 kHz.

Resonance Raman Spectroscopy. Resonance Raman spectra were recorded using a spectrometer comprising a 0.6 m spectrograph equipped with a 2400 groove/mm grating and a LN2 cooled CCD detector. Raman excitation was achieved with the 406.7 nm emission line from a Kr^+ laser, focused to a line on the sample. Scattered light was collected using an *f*1 lens, filtered through a holographic notch filter to remove Rayleigh scattered light, and passed through a polarization scrambler. Samples were contained in a 5 mm NMR tube spun at ~20 Hz during data acquisition. Spectra were calibrated against the known Raman frequencies of toluene and dimethylformamide bands.

Circular Dichroism Spectroscopy. CD spectra were recorded at 25 °C on a Jasco J-710 spectropolarimeter equipped with a Neslab RTE-111 circulating water bath and a Neslab RS232 remote temperature sensor. A 1.0 cm cylindrical, water-jacketed cell was used in all cases. Far-UV spectra (sample concentration 1.8−2.5 μM) are reported in terms of mean residue ellipticity ([θ], in deg·cm^2·dmol^{-1}), calculated as $[\theta] = [\theta]_{obs}(MRW/10lc)$, where $[\theta]_{obs}$ is the ellipticity measured in millidegrees, MRW is the peptide mean residue molecular weight (molecular weight divided by the number of amino acids), c = sample concentration in mg/mL, and l = optical path length of the cell in cm. Soret region spectra (sample concentration 10−12 μM) are reported in terms of molar ellipticity ([θ]$_{Soret}$, in deg·cm^2·dmol^{-1}), calculated as $[\theta] = [\theta]_{Soret}(MW/10lc)$, where MW is the molecular weight of the compound. All spectra represent an average of five scans. The peptide helix content for **2** was determined as described previously (*41*). Data from the imidazole binding titration monitored by CD spectroscopy were analyzed using the appropriate variant of eq 1.

pH Titrations. pH titrations were performed on the Uvikon spectrophotometer and Jasco spectropolarimeter described above. We used the multicomponent buffer system developed by Munro and Marques for examining the pH-dependent behavior of **1** (*12*), comprising CHES, MES, MOPS, potassium hydrogen phthalate, and Tris (each at 1.0 mM), at a total ionic strength of 0.10 M (KCl). Samples of **1** and **2** (2−3 μM) contained a total volume of 3.0 mL and included 40% (v/v) CH_3OH to prevent aggregation. The pH was adjusted from pH ~8 to pH 1.5 in approximately 0.2 pH increments by adding 1 M HCl. The solution was allowed to equilibrate at each pH for 5 min. For determination of spectroscopic pK_a's by CD, we monitored the ellipticity (θ) at 222 nm (for **2**) or 396 nm (for **1**). Each data point was obtained by averaging the signal intensity at the desired wavelength over a period of 5 min. The pK_a values were determined (Igor Pro, v.4.0; Wavemetrics, Inc.) using eq 2,

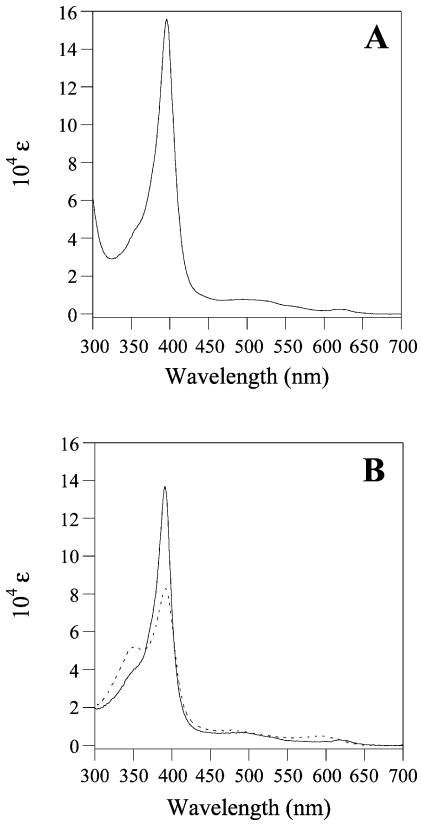

FIGURE 1: (A) Electronic absorption spectrum of **1** in aqueous solution. (B) Electronic absorption spectrum of **2** in aqueous solution (---) and in 60:40 H_2O/CH_3OH (—). All spectra were recorded at 25 °C, and solutions were buffered to pH 8.0 with 50 mM potassium phosphate.

$$\theta_{pH} = \frac{\theta_{pH1.5} + \theta_{pH6.5} n(pK_a - pH)}{1 + 10^{n(pK_a - pH)}} \quad (2)$$

where θ_{pH} is the ellipticity at a given pH, $\theta_{pH1.5}$ is the ellipticity at pH 1.5 (representing the His-dissociated form of the compound), $\theta_{pH6.5}$ is the ellipticity at pH 6.5 (representing the His-ligated form of the compound), pK_a is the transition midpoint, and n is the number of protons involved in the transition.

RESULTS AND DISCUSSION

Effect of Structure on Self-Association. Although **1** and **2** both dissolve readily in water, their properties are clearly different as evidenced in electronic absorption spectra. In the spectrum of **1** at pH 8.0 (Figure 1A), the Soret band λ_{max} is located at 396 nm, the high-spin β-band (Q_v) is near 495 nm, and a porphyrin π to iron charge transfer band appears at 620 nm. The spectrum is suggestive of a predominantly high-spin, monomeric ferric porphyrin, as previously reported (*12*, *17*). In contrast, the corresponding spectrum of **2** (Figure 1B) exhibits features inconsistent with a monomeric porphyrin. Most notable are the severe hypochromism of the Soret band of **2** relative to **1** and the presence of a broad band near 350 nm, which provide evidence of $\pi-\pi$ stacking interactions (*42*). These features disappear when methanol (40 vol %) is included as a cosolvent (Figure

1B). Beer's law plots (Figure S1, Supporting Information) show that **1** is monomeric over a wide concentration range in this solvent but that **2** is monomeric only at concentrations below 15 μM. In the spectrum of monomeric **2**, the Soret band (λ_{max} = 391 nm) and Q-band (λ_{max} = 491 nm) occur 4−5 nm to the blue of the same bands in the spectrum of **1**.

The tendency of **2** to self-associate more readily than **1** is noteworthy, considering that one face of heme is solvent exposed in both compounds. As noted above, heme in **1** exhibits a ruffled conformation, but RR data presented herein indicate less extensive ruffling in **2**. A planar heme is more likely to dimerize via $\pi-\pi$ stacking, because a greater extent of surface area can come into contact in the dimer. In fact, $\pi-\pi$ stacking has been shown to induce planar conformations in nickel(II) uroporphyrins (*43*). We propose that the smaller degree of heme ruffling in **2** is the most likely source of its greater tendency to aggregate. Self-association of **1** may be further disfavored electrostatically, as its heme contains two negatively charged propionate groups rather than one.

Peptide Secondary Structure. CD spectroscopy provides useful information about peptide conformation (*44*). A fully helical peptide exhibits a negative band in the vicinity of 220−222 nm, corresponding to amide n−π* transitions, and a negative band of similar intensity near 208 nm and a strong positive band near 190 nm resulting from exciton coupling of amide $\pi-\pi$* transitions. The dominant feature in randomly structured peptides is a band with a negative Cotton effect near 200 nm. The far-UV CD spectrum of **1** in 60:40 (v/v) H_2O/CH_3OH, pH 8.0 (Figure S2A, Supporting Information), displays a negative band near 201 nm and a less intense negative band near 220 nm. These features suggest some degree of helical secondary structure, consistent with published NMR studies (*20*). The corresponding spectrum of **2** (Figure S2B) indicates that the peptide exhibits approximately 50% helix content (averaged across all residues). The asymmetric environment provided by the peptide chain in **1** results in CD signals arising from heme electronic transitions. A CD Soret band with a strong, positive Cotton effect is observed for **1** at 396 nm (Figure S2A) (*45*, *46*). The corresponding signal in the spectrum of **2** exhibits a negative Cotton effect and is centered at 391 nm (Figure S2B).

Peptide Secondary Structure Requires an Intact His to Iron Bond. Munro and Marques have reported that the electronic absorption spectrum of **1** is largely independent of pH over the range of 6−8 in aqueous solution (*12*). As the pH is lowered from 6 to 4, the intensity of the Soret band λ_{max} decreases but remains centered at 396 nm, changes attributed to protonation of the heme propionate groups (pK_a = 6.1 and 4.95) (*12*). Decreasing the pH from 4 to 2 results in enhanced intensity of the Soret band and a λ_{max} shift from 396 to 393 nm, which results from dissociation/protonation of the His ligand (pK_{obs} = 3.12) (*12*). We performed an independent pH titration of **1** in 60:40 H_2O/CH_3OH, monitored by electronic absorption spectroscopy, and obtained essentially identical results (see Figure S3A, Supporting Information).

A CD spectrum of **1** recorded at pH 1.5 (Figure S2A) reveals that the signal centered near 220 nm has disappeared. The resulting spectrum is characteristic of a peptide with a random coil conformation (*44*). In addition, the CD Soret signal of **1** has essentially disappeared from the spectrum at pH 1.5. Shelnutt and co-workers have presented evidence that His dissociation in cyt *c* heme peptides in aqueous solution weakens the hydrogen-bonding interactions that stabilize the helical turn between residues 14 and 17 and that it diminishes heme ruffling (*21*, *47*). The latter effect has experimental support (*16*). Our CD studies show, for the first time, that His dissociation in **1** actually results in complete disruption of peptide secondary structure.

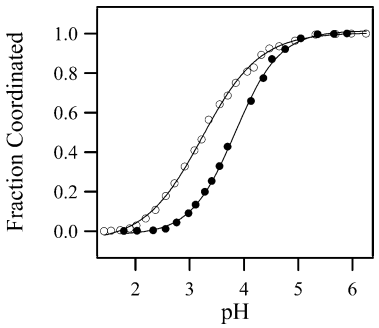

FIGURE 2: Normalized data from pH titrations of **1** (open circles) and **2** (closed circles) at 25 °C monitored by CD spectroscopy (see text for details). The solid lines through the points represent fits of the data to eq 2.

The electronic absorption spectrum of **2** is also largely independent of pH in the range of 6−8. Lowering the pH from 6 to 5 does not significantly diminish Soret band intensity as occurred with **1**, but a small increase in extinction coefficient occurs as the pH is lowered from pH 5 to pH 3 with a concomitant shift of λ_{max} from 391 to 389 nm (Figure S3B). The blue shift over this pH range suggests dissociation of the axial His ligand. Consistent with this possibility, a CD spectrum of **2** recorded at pH 1.5 reveals that its peptide is also random coil and that the CD Soret band signal has disappeared (Figure S2B).

*His−Fe(III) Coordination Is Stronger in **1**.* We took advantage of the large changes in CD spectra of **1** and **2** upon His dissociation to determine equilibrium constants for the process via pH titrations to compare His−Fe(III) coordination strengths. The values of K_{app} determined in such experiments represent two steps: deprotonation of $HisH^+$ followed by coordination of His to Fe(III) (eq 3; K_{app} =

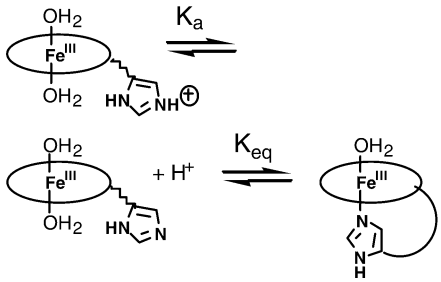

(3)

K_aK_{eq}). For the pH titrations of **1** and **2**, we monitored changes in CD Soret band intensity and in ellipticity at 220 nm, respectively. Fits of the data to eq 2 (Figure 2) yielded the data in Table 1. The value of pK_{app} determined for **1** using this method (3.26) is similar to the value determined by Munro and Marques in spectrophotometric experiments (3.12) (*12*). The pK_{app} value determined for **2** is ∼0.6 pH unit higher. These values correspond to a free energy change upon acid-induced His dissociation ($\Delta G°_{app}$) that is 0.7 kcal/

Table 1: Data from pH Titrations of **1** and **2** at 25 °C

	pK_{app}	n	K_{app}[a] (M^{-1})	K_{eq}[a]	$\Delta G°_{eq}$[a] (kcal/mol)
1	3.26	0.92	5.50×10^{-4}	1718	−4.4
2	3.83	1.09	1.48×10^{-4}	462	−3.7

[a] Calculated using the assumption that the dissociated His ligands in **1** and **2** have identical pK_a values (see text).

mol less favorable in the case of **1**. The data suggest that the His ligand in **1** is coordinated to iron approximately 4-fold more strongly than the His ligand in **2**. Using a typical acid dissociation constant for $HisH^+$ (pK_a = 6.5), we can calculate approximate values of K_{eq} (Table 1). These should be considered as approximations, because differences in the microenvironments of $HisH^+$ in His-dissociated **1** and **2** may cause their pK_a values to differ.

Even though His dissociation in **1** triggers unwinding of the helix defined by residues 14−17, the double heme−peptide attachment is expected to severely limit its conformational flexibility (*8*). In addition, because only a single residue separates His-18 in **1** from its covalent linkage to heme, it cannot wander far from iron even when the 14−17 helix unwinds. In contrast, the peptide in **2** is connected to heme via a single flexible linker, and three amino acid residues separate the covalently attached Lys residue from His. We therefore expect that His dissociation should be entropically more favorable in **2** than in **1**. The stronger His coordination by **1** evidenced in pH titrations is consistent with these considerations.

*Source of the Red-Shifted Soret and Q-Bands of **1***. The Soret and Q-bands in the electronic absorption spectrum of His-dissociated **1** are red shifted relative to the bands of His-dissociated **2** by 4−5 nm. The red shifts are essentially of the same magnitude as in the corresponding His-coordinated forms. One possible source of such a red shift is a greater degree of heme ruffling in **1** relative to **2** (*49*). As already noted, cyt *c* heme peptides maintain some of the heme ruffling exhibited by the parent protein. The extent of ruffling diminishes when the axial His ligand dissociates, which we have shown to be accompanied by loss of peptide secondary structure. Consistent with these reports, RR data reported herein (vide infra) indicate that the heme is more ruffled in **1** than in **2**. In fact, heme ruffling is rare in unstrained high-spin ferric porphyrins (*50*), leading us to predict that the heme in **2** will be largely planar in both the His-ligated and His-dissociated forms. The fact that the extent of the red shifts of the Soret and Q-bands of **1** relative to **2** does not diminish significantly upon dissociation of the axial His ligands therefore suggests that heme ruffling is not the principal source of the effect. This is consistent with a recent report showing that Soret and Q-bands of metalloporphyrins are only marginally affected by distortion until the porphyrin atoms are displaced by more than 1.0 Å from the mean plane (averaged over all atoms) (*49*). The extent of ruffling calculated for the His-ligated form of **1** with the fully helical peptide (∼0.7 Å) (*21*) is less than this value. A more likely source of the red-shifted bands of **1** relative to **2** is the only significant difference in their heme substituents: the $-CH(SR)CH_3$ moieties of **1** versus the corresponding $-CH_2CH_3$ groups in **2**. Because sulfur is similar in electronegativity to hydrogen, the effect cannot be due to differences in electron withdrawal or electron donation arising from these substituents. We propose that perturbation of the porphyrin molecular orbitals by the C−S bonds of **1** (via hyperconjugation) is the primary source of its red-shifted bands.

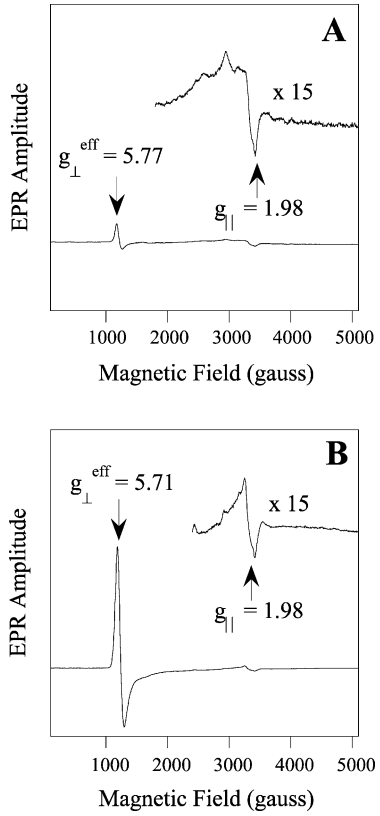

FIGURE 3: EPR spectra of **1** (A) and **2** (B) recorded at 11 K in 3:1:1 water/methanol/glycerol buffered to pH 8.0 with 100 mM potassium phosphate.

*Evidence for a Stronger Ligand Field in **1***. EPR spectra of **1** and **2** recorded at 11 K are shown in panels A and B of Figure 3, respectively. The spectrum of **1**, with $g_\perp \approx 5.7$ and $g_{||} = 1.98$ and with additional intensity between $g = 2$ and $g = 3$, is similar to previously published spectra (*51*, *52*). The $g_\perp$ value, suggestive of axially distorted high-spin Fe(III) (*53*), is somewhat low for purely high-spin iron. Munro et al. have shown that this is indicative of a quantum mechanically admixed high-spin/intermediate-spin ($S = {}^5/_2$, ${}^3/_2$) state (*52*). This form is in thermal equilibrium with a low-spin ($S = {}^1/_2$) form, which is the source of the EPR intensity between $g = 2$ and $g = 3$ (*52*). In the spectrum of **2**, the $g_\perp$ signal occurs at higher field and is somewhat broader than in **1**. These features suggest a slightly greater contribution of $S = {}^3/_2$ iron to the signal, indicative of a weaker ligand field in **2** than in **1**. For simplicity, we will hereafter refer to this form of iron in both **1** and **2** as high spin. The axial signals are reproducibly much less intense in the spectrum of **1** than in the spectrum of **2**. Furthermore, the additional signals between $g = 2$ and $g = 3$ in the spectrum of **1** are less intense in the spectrum of **2**, indicating that Fe(III) in **2** exhibits a smaller degree of low-spin character at 11 K. This provides further evidence that the ligand field experienced by Fe(III) in **2**, comprising the heme and the axial His and aquo ligands, is weaker than in **1**.

RR spectra of **1** and **2** in 1:1 (v/v) H_2O/CH_3OH (pH 7.0, 25 °C), with Soret band excitation at 406.7 nm, are shown

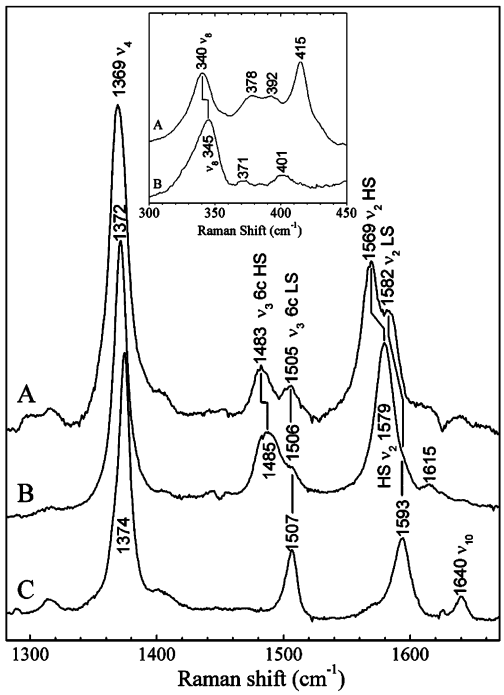

FIGURE 4: High-frequency resonance Raman spectra of **1** (A), **2** (B), and **3** (C) with Soret band excitation at 406.7 nm. The inset shows a portion of the corresponding low-frequency spectra of **1** and **2**. All spectra were recorded at 25 °C in 1:1 H_2O/CH_3OH buffered to pH 7.0 with 50 mM sodium phosphate. Laser power at the sample ranged from 14 to 20 mW.

in Figure 4. Also included in Figure 4 is the RR spectrum of the low-spin bispeptide analogue of **2** (**3**) (*54*). The oxidation state marker bands (ν_4) in the spectra of **1** and **2** are at 1369 and 1372 cm^{-1}, respectively, indicative of hexacoordinated Fe(III) in each case. Two ν_3 (spin state marker) bands are present in the spectra of **1** and **2** as well. The bands at lower frequency (1483 cm^{-1} for **1**; 1485 cm^{-1} for **2**) are attributable to hexacoordinate, high-spin Fe(III), while the bands at higher frequency (1505 cm^{-1} for **1**; ∼1506 cm^{-1} for **2**) arise from the low-spin forms. Consistent with this latter assignment, ν_3 in the spectrum of low-spin **3** is located at 1507 cm^{-1}. There are also two distinct ν_2 bands in the spectrum of **1**, at 1569 and 1582 cm^{-1}. These have been identified as arising from high-spin and low-spin Fe(III), respectively (*17*). The corresponding bands in the spectrum of **2** are at 1579 and ∼1593 cm^{-1} (shoulder). The occurrence of ν_2 at 1593 cm^{-1} in the spectrum of **3** confirms this latter assignment. These data are consistent with Fe(III) in both **1** and **2** exhibiting a thermal high-spin/low-spin equilibrium, as previously reported for **1**. It should be noted that the excitation wavelength used in these experiments (406.7 nm) will likely provide greater relative resonance enhancement for the low-spin component ($\lambda_{max} \sim 402-408$ nm) than for the high-spin component (Soret band $\lambda_{max} =$ 396 nm for **1** and 391 nm for **2**), tending to exaggerate contributions due to the low-spin form. The fact that the signals corresponding to low-spin Fe(III) are less prominent in the spectrum of **2** than in the spectrum of **1** is consistent with a smaller contribution of the low-spin form in **2**. It must be considered, however, that the red-shifted Soret band of **1** relative to **2** results in **1** exhibiting a significantly higher extinction coefficient from the high-spin form at the excitation wavelength of 406.7 nm (Figure S4, Supporting Information). We expect this to result in greater prominence of the low-spin features in the spectrum of **2** than in the case of **1**. Hence, the high-spin/low-spin population ratio for **1** exceeds that for **2** by an amount greater than is apparent from casual comparison of the relative band intensities in Figure 4. The RR data therefore support the conclusion that Fe(III) experiences a considerably stronger ligand field in **1** than in **2**.

Chart 2

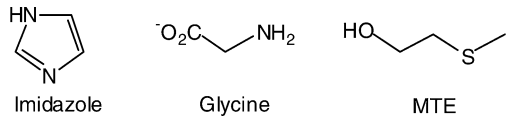

*Heme Is More Ruffled in **1***. Many bands in RR spectra of metalloporphyrins are sensitive to out-of-plane porphyrin deformations (*55*), including ν_2, ν_3, ν_4, and ν_8 (*47*). The ν_3 and ν_4 band frequencies are insensitive to changes in heme substituents, making them useful indicators of differences in heme ruffling between **1** and **2**. Out-of-plane distortions are generally manifested as lower frequency ring-stretching vibrations. The fact that the ν_3 and ν_4 bands in the spectrum of **1** are centered at lower frequencies than their counterparts in the spectrum of **2** therefore suggests that heme in **2** exhibits a less ruffled conformation, consistent with its less strained, solitary heme−peptide linkage.

Binding Studies with Ligands Representing Amino Acid Side Chains. For an initial comparison of the ligand binding properties of **1** and **2** we chose to examine three ligands representing analogues of amino acid side chains which coordinate trans to His in natural heme proteins (Chart 2). Complexes formed with imidazole, an analogue of the His side chain, would mimic the coordination geometry of bis-His coordinated heme proteins such as cyt b_5. Glycine serves as an analogue of the protein N-terminus, which is coordinated trans to His in the CO-binding transcription factor CooA (*56*) and in cyt *f* (*57*). It can also represent the side chain of lysine, which replaces Met-80 in cyt *c* at high pH (the alkaline form of cyt *c*) (*58*, *59*). Finally, 2-(methylthio)-ethanol (MTE) represents the thioether side chain of Met (*60*). Coordination of the MTE sulfur atom to **1** and **2** would yield complexes that mimic the axial coordination environment of cyt *c*. We chose to use MTE as an analogue of the Met side chain rather than the more commonly employed *N*-acetylmethionine (AcMet), because AcMet has a maximum solubility of ∼2 M in buffered aqueous solution (*17*, *60*). Hence, only about 75% saturation binding of **1** can be achieved with AcMet (*10*, *17*). Using unbuffered solutions in titrations with MTE, we are able to achieve >95% saturation binding of **1** (*60*).

Binding of Imidazole and Glycine. Titrations of **1** and **2** with imidazole and glycine were performed in 60:40 H_2O/CH_3OH buffered to pH 8.0 with 50 mM potassium phosphate. In each case, the Soret band shifted 8−11 nm to longer wavelength (Table 2 and Figures S5−S8, Supporting Information), consistent with a high-spin to low-spin transition of iron. Changes in the visible region of the spectrum were also consistent with such a conversion. Most notably, the π to iron charge transfer band centered near 620 nm disappears in each titration. After correcting for the pK_a value of the ligand, we find that imidazole has modestly higher affinity for both heme peptides than does glycine (Table 2). The

Table 2: Data from Ligand Binding Titrations of **1** and **2** at 25 °C

	K_a (L/mol)		$\Delta G°$ (kcal/mol)		λ_{max} (nm)	
	1	**2**	**1**	**2**	**1**	**2**
H_2O					396	391
ImH[a,c]	6254	7728	−5.3	−5.5	405	402
ImH[b,c]	0.2	1.8	+1.0	−0.4		
glycine[d]	941	615	−4.0	−3.8	404	400
MTE	1.2	0.6	−0.2	+0.3	408	394

[a] First equivalent of imidazole, displacing the aquo ligand. [b] Second equivalent of imidazole, displacing the axial His ligand. [c] Adjusted for the pK_a of imidazole (7.00). [d] Adjusted for the pK_a of glycine (9.70).

association constants we obtained for binding of imidazole and glycine by **1** closely match values that have previously been reported (*17*, *61*). Each of these ligands binds to **1** and **2** with nearly equal affinity.

Displacement of His by Imidazole. It has been reported that His-18 in the low-spin imidazole complex of **1** can be displaced by imidazole, yielding a low-spin bisimidazole complex (eq 4) (*16*). We have shown that displacing His in

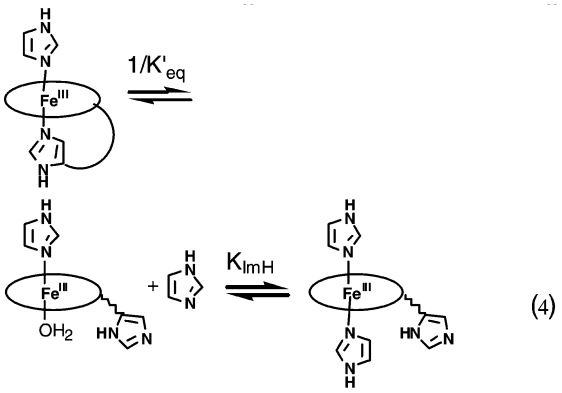

(4)

1 and **2** is accompanied by loss of the CD Soret band signal. This reaction therefore offers an alternative means of comparing His−Fe(III) coordination strength in **1** and **2**. Increasing the imidazole concentration above that required to achieve >95% of the imidazole/histidine-coordinated complex at pH 8.0 results in gradual disappearance of the CD Soret band signal in each case. A higher imidazole concentration was required to effect His displacement in **1** than in **2** (Table 2), indicating stronger coordination of His in **1**. In fact, displacement of His by imidazole in **1** is endergonic by 1 kcal/mol, while displacement of His in **2** is slightly exergonic. Association constants obtained by fits of the data to eq 1 (Table 2 and Figure S11) equal the product of the two equilibrium constants in eq 4 ($K_{obs} = K_{ImH}/K'_{eq}$). On the assumption that K_{ImH} is identical for **1** and **2**, the results indicate that His coordinates to iron 9-fold (1.4 kcal/mol) more strongly in **1** (Table 2), a difference twice as large as that estimated in the pH titrations described above (Table 1). The difference in K_{obs} for **1** and **2** determined by eq 4 is less dependent on the pK_a of the dissociated His ligands than is the difference in K_{app} determined from eq 3. Hence, the 1.4 kcal/mol difference in His coordination strength estimated using eq 4 is probably closer to the actual value.

Binding of MTE. Data from titrations of **1** and **2** with MTE are shown in panels A and B of Figure 5, respectively. Coordination of MTE by **1** is accompanied by a 12 nm shift of the Soret band λ_{max}, consistent with the expected conversion of iron from the high-spin to the low-spin form. Changes in the visible region of the spectrum are also indicative of such a change. Notably, we observe a weak band near 695 nm in the spectrum of the MTE complex. A similar band has been observed in spectra of other thioether complexes of cyt *c* heme peptides (*17*, *27*, *60*), as well as in cyt *c* itself (*62*, *63*), and is considered to be diagnostic of thioether coordination. Consistent with previous reports (*17*, *27*, *60*), coordination of MTE by **1** is only slightly exergonic, indicating that it is only modestly stronger than water as a ligand to Fe(III).

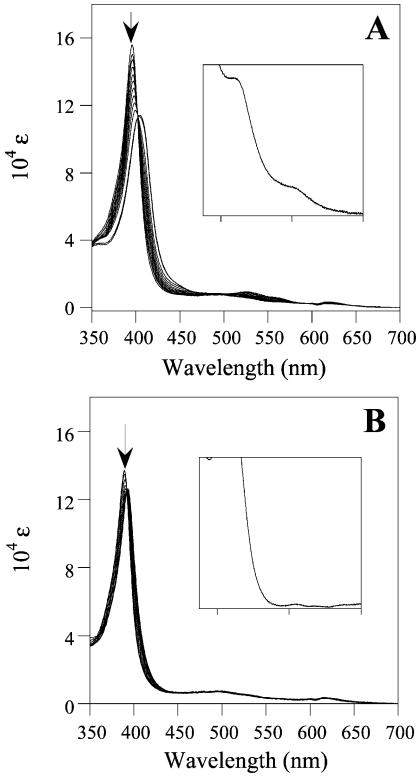

FIGURE 5: Data from binding titrations of **1** (A) and **2** (B) with MTE in 60:40 H_2O/CH_3OH.

Binding of MTE by **2** results in much smaller changes in its electronic absorption spectrum than observed for **1** (Figure 5B). The Soret band λ_{max} shifts only 3 nm to the red (Table 2) during the titration, only minor changes occur in the visible region of the spectrum, and no band appears near 695 nm. Nonetheless, isosbestic points and saturation behavior are observed. Fitting of the binding data shows that complexation of MTE by **2** is endergonic, with binding approximately 0.5 kcal/mol less favorable than in the case of **1**. Furthermore, the data indicate that MTE binding by **2** does not trigger conversion of iron to the low-spin state, contrary to our initial expectations and in marked contrast to its effect on the spin state of **1**. Almost identical changes in the spectrum of **2** are observed in the presence of a high concentration of dimethyl sulfide (in methanol solution), indicating that the failure to observe a low-spin complex with MTE does not derive from preferential coordination of its hydroxyl oxygen atom.

On the basis of changes in the visible spectrum of **1** in its titration with MTE, we expect that it should be possible to detect a low-spin population in the corresponding titration with **2** if it constitutes ≥10% of the total sample. We can therefore safely conclude that the MTE complex of **2** is greater than 90% high-spin under the conditions used in the

titration. Hence, the $S = {}^1/_2$ state in the MTE complex of **2** is *destabilized* relative to the $S = {}^5/_2$ state by at least 1.3 kcal/mol under the conditions used in the titration. Making the conservative assumption that iron in the MTE complex of **1** is 90% low spin under the binding titration conditions, the $S = {}^1/_2$ state is *stabilized* relative to the $S = {}^5/_2$ state by at least 1.3 kcal/mol.

*Stabilizing the Low-Spin State in the MTE Complex of **2**.* We have shown that His coordinates to Fe(III) ~1.4 kcal/mol more strongly in **1** than in **2**, a result of greater constraints imposed on its peptide conformation by the double covalent heme−peptide linkage. In addition, **1** binds MTE 0.5 kcal/mol more strongly than does **2**. Thus, the total free energy of His and MTE binding is ~1.9 kcal/mol more exergonic for **1** than for **2**. It is possible that this is the source of the stronger ligand field experienced by Fe(III) in the MTE complex of **1**.

Formation of bimolecular complexes is typically more energetically favorable at lower temperatures, due to a less negative $T\Delta S°$ term. For example, the free energy of MTE binding by the Fe(II) complex of **1** becomes more favorable by approximately 0.8 kcal/mol upon decreasing the temperature from 45 to 25 °C (*60*). A lower temperature should also favor stronger coordination of the intramolecular His ligand. That this is the case is suggested by studies of the Fe(II) form of **3**, which exhibits an equilibrium between bis-His and mono-His coordination (*64*). The ratio of bis-His to mono-His coordination in Fe(II)−**3** increases from ~1:1 to ~3:1 as the temperature is lowered from 35 to 15 °C, representing an increase in stability of the His−Fe(II) bond of approximately 0.6 kcal/mol.

Spectra of **2** recorded at 25, 15, and 5 °C in 90:10 (v/v) H_2O/CH_3OH in the presence of 2.8 M MTE at pH 8.0 reveal a decrease in intensity of the Soret band λ_{max} at 393 nm and the appearance of a small shoulder on the long-wavelength side of the Soret band. These changes suggest the emergence of low-spin iron in equilibrium with the predominant high-spin form. We also observed changes in the visible region of the spectrum suggesting the appearance of low-spin iron, including decreased intensity of the π−iron charge transfer band. We subsequently discovered that combining the temperature change with an increase in solvent polarity (by increasing the ratio of water to methanol) exerted an even greater effect, most likely by favoring stronger binding of MTE via a hydrophobic effect. Spectra of the MTE complex of **2** recorded at 25 °C in 60:40 H_2O/CH_3OH and at 5 °C in 90:10 H_2O/CH_3OH are shown in Figure 6. The signal for low-spin iron in the latter spectrum is clearly evident, with $\lambda_{max} \approx 403$ nm, still as a shoulder on the Soret band for the high-spin form. We also observe a weak signal near 695 nm, providing further evidence for the presence of a low-spin thioether complex. Comparing the latter spectrum with data from the MTE titration of **1**, we estimate that the MTE complex of **2** exhibits at least 50% low-spin character under the most favorable conditions examined. In other words, changing the conditions has pushed the complex close to, and perhaps beyond, the spin crossover point. The results of these experiments support the conjecture that the stronger ligand field experienced by Fe(III) in the MTE complex of **1** in comparison to the corresponding complex of **2** arises from thermodynamically more favorable coordination of the intramolecular and exogenous axial ligands.

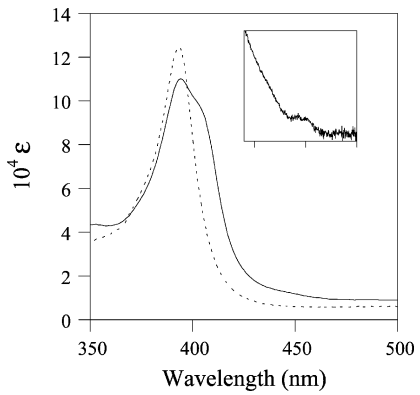

FIGURE 6: Electronic absorption spectra of the complex between MTE (2.8 M) and **2** (8 μM) at pH 8.0. Dashed line: 60:40 H_2O/CH_3OH at 25 °C. Solid line: 90:10 H_2O/CH_3OH at 5 °C.

*Other Potential Sources of the Stronger Ligand Field in **1**.* A stronger ligand field in **1** might occur if the Nδ1 proton of His-18 engages in a hydrogen-bonding interaction that endows it with histidinate (His^-) character absent in **2**. It has been proposed that the conserved hydrogen bond between the backbone carbonyl oxygen of Pro-30 and the His-18 Nδ1 proton in cyt *c* plays such a role (*65*, *66*). The strongest available bases in **1** are the two heme propionates and the α- and γ-carboxylate groups of Glu-21. The pH titrations described above indicate that at pH 4.5 one of the heme propionates in the MTE complex of **1** should be fully protonated and the other should be >50% protonated. The α- and γ-carboxylate groups of Glu-21 should also be at least partially protonated at pH 4.5. Electronic absorption spectra of the MTE complex of **1** recorded at pH 8 and at pH 4.5 are essentially identical, ruling out the possibility that any of these groups contributes to the low-spin state of Fe(III) at pH 8.

We have noted that the $-CH(SR)CH_3$ moieties of **1** perturb its porphyrin molecular orbitals relative to the $-CH_2CH_3$ groups in **2**, resulting in red-shifted Soret and Q-bands. The similar electronegativities of sulfur and hydrogen render it highly unlikely that they alter the ligand field of the porphyrin by changing the electron-donating properties of its central nitrogen atoms. However, it is possible that perturbation of the porphyrin molecular orbitals by the thioether substituents of **1** affects the interactions between the porphyrin orbitals and the d_{xz} and d_{yz} orbitals of iron (*67*). This factor could conceivably alter its ligand field strength. We consider it unlikely that such a small difference in porphyrin electronic sructure would exert an effect on its ligand field strength of the magnitude observed here, but it cannot be ruled out as a contributing factor. Another factor that cannot be ruled out is heme ruffling, induced by His−Fe(III) coordination in **1** but less prominent in **2** as evidenced in RR spectra. Examining possible roles played by heme ruffling in **1** and **2** will be the focus of future studies.

Implications for Identification of His−Met Coordination in Other Systems. Prior to identification of Met as the second axial heme ligand in ferric cyt *c* via studies with microperoxidase-8, it was believed that the low affinity of thioethers for Fe(III) would prevent Met from playing such a role (*27*, *62*). The ubiquity of low-spin His−Met coordination in the cyt *c* family has perhaps led to the expectation that all ferric porphyrins exhibiting imidazole/thioether coordination should

be low spin, despite the paucity of other examples in the literature besides thioether-coordinated cyt *c* heme peptides such as **1** and the proteins cyt b_{562} and Dos discussed below. It has been argued that the failure to observe His−Met coordination in synthetic ferric porphyrins is due to the inability of thioethers to displace anionic ligands in the organic solvents that are employed (*28*, *30*). These conclusions are typically based on the absence of spectroscopic signatures characteristic of cyt *c*, namely, low-spin iron and a ligand to metal charge transfer band near 695 nm. Using synthetic heme peptide **2**, which shares many features with cyt *c* heme peptides including solubility in polar protic solvents, we have demonstrated that the combination of an imidazolyl moiety and a thioether does not present a sufficiently strong ligand field to guarantee a low-spin state for a ferric porphyrin. Hence, the spectroscopic signatures of cyt *c* will not always be useful for identifying or verifying His−Met coordination in natural, engineered, or de novo designed heme proteins nor in synthetic heme peptides or other cyt *c* models.

Proposed Roles for the Double Covalent Heme−Protein Linkage in Cyt c. Coordination of His-18 to Fe(III) in acid-denatured cyt *c* triggers folding of the initially random coil protein (*68*). Met-80 does not participate in the folding reaction. Likewise, we have found that His−Fe(III) coordination in **1** and **2** induces folding of a random coil peptide and that the reaction is ∼1.4 kcal/mol more energetically favorable in the case of **1**. We have attributed this to the greater conformational constraints imposed on the peptide in the His-dissociated form of **1** than in the corresponding form of **2**, a result of its double covalent heme−peptide linkage. This is consistent with a recent report showing that elimination of the covalent linkage between Cys-14 and heme in yeast cyt *c* destabilizes the protein fold (*7*).

That the ligand field presented to Fe(III) is stronger in the aquo complex of **1** than in the corresponding complex of **2** is surprising, considering that the ligand set (porphyrin, His, and H_2O) is essentially identical in the two complexes. For the same reason, we did not anticipate that only in the case of **1** would displacement of water by MTE trigger conversion of Fe(III) to the low-spin configuration characteristic of cyt *c*. As noted above, this demonstrates that the ligand field provided by one imidazole and one thioether is too weak to guarantee a low-spin configuration for a ferric porphyrin. Cyt *c* has clearly evolved a solution for circumventing this limitation, which is also manifested in proteolytic fragments of cyt *c* such as **1**. We propose that the thermodynamically more favorable His−Fe(III) coordination in **1** and in cyt *c* enabled by their double covalent heme−protein linkages magnifies the intrinsic ligand field strength of His. This represents a previously unrecognized role played by the heme−protein linkage in cyt *c*.

As noted in the introduction, formation of the Met−Fe(III) bond in cyt *c* appears to require the preorganization offered in an already folded protein. Our titrations of **1** and **2** with MTE highlight the need for such preorganization by confirming the inherently poor affinity of thioethers for ferric porphyrins. However, these studies led to the unexpected finding that **1** binds MTE more strongly than does **2**, with the reaction endergonic in the latter case. Although the reasons for the stronger affinity of **1** for MTE have not yet been elucidated, it clearly is a consequence of the two-point covalent attachment of heme to protein in **1**. Hence, the double covalent heme−protein linkage in cyt *c* may likewise enable stronger coordination of Met-80 than would be possible if only a single linkage were present. In addition to further stabilizing the protein fold, this may also enhance the effective ligand field strength of Met-80. This possibility is supported by the observation that conditions favoring stronger coordination of both His and Met to **2** (lower temperatures, greater solvent polarity) increase the low-spin character of the complex.

Importance of Preorganization for His−Met Coordination. His−Met-coordinated heme proteins are rare outside of the cyt *c* family. The best known example is cyt b_{562}, a four-helix bundle protein from *Escherichia coli* containing reversibly bound heme (*69*). EPR (*70*) and RR (*71*) studies have characterized Fe(III) in cyt b_{562} as low spin, but NMR studies have shown that the protein exhibits a thermal $S = {}^1/_2, {}^5/_2$ equilibrium with low spin predominating (∼14% high-spin content at 45 °C) (*72*). In contrast, $S > {}^1/_2$ spin states are rarely thermally accessible in His−Met-coordinated cyt *c*. These data indicate that low-spin iron is stabilized relative to the high-spin state to a lesser extent in ferric cyt b_{562} than it is in ferric cyt *c*, showing that the ligand field experienced by Fe(III) in this protein is weaker than in cyt *c*.

In striking contrast to cyt *c*, heme dissociation from cyt b_{562} does not result in protein unfolding. Rather, three of the four helices in the cyt b_{562} helix bundle remain largely intact, including the helix containing the Met ligand (*73*, *74*). Hence, a smaller percentage of the heme binding energy is expended to organize the protein structure in ferric cyt b_{562} than in the case of ferric heme binding to apocyt *c*. This suggests that preorganizing the heme binding site in an apoprotein represents another useful mechanism that nature has evolved for stabilizing low-spin His−Met coordination but one that is not quite as effective as the conformationally restricted heme−protein covalent linkage of cyt *c*. Further preorganizing cyt b_{562} by engineering a covalent link between a Cys side chain and heme yields a mutant that is stabilized toward unfolding (*75*). The modification also enhances the ligand field strength experienced by Fe(III) as evidenced by the fact that low-spin character is greater in the mutant than in the wild-type protein (*76*). This is consistent with our observation that ligand field strength in **1** and **2** increases as the ligand binding free energy becomes more favorable.

A more recently described *b*-type heme protein exhibiting His−Met coordination is the O_2 sensor Dos, also from *E. coli* (*77*). Ferric Dos exhibits approximately 10% high-spin iron at room temperature, apparently arising from both Met-ligated and Met-dissociated forms. Although no data have yet been published regarding the apo form of Dos, we predict that like cyt b_{562} it contains a well-organized heme binding site.

It is noteworthy that the only reported attempts to engineer His−Met coordination into *b*-type heme proteins have been unsuccessful. Sligar et al. (*78*) mutated heme ligand His-39 in rat microsomal cyt b_5 to Met. RR spectra indicated that the ferric protein exhibited high-spin, six-coordinate iron, but the authors did not determine whether the axial ligand trans to His-63 was the engineered Met or water. Rodriguez and Rivera replaced His-63 in rat outer mitochondrial membrane cyt b_5 with Met (*79*). This mutant also exhibited six-coordinate high-spin Fe(III), but NMR studies demon-

strated that Met was not coordinated trans to His-39. Heme loss from cyt b_5 results in substantial disruption of secondary structure comprising the heme binding pocket, although the protein remains folded (*80*). The surprising failure to observe His−Met coordination in these cyt b_5 mutants suggests that too much of the heme binding energy is expended in refolding of local structure, as in the case of ferric heme binding to apocyt *c*, thus preventing Met−Fe(III) coordination. These results highlight the difficulties that will be faced in engineering or designing His−Met coordination in heme proteins.

Finally, we note two unusual members of the cyt *c* family, cyt c_{557} from *Crithidia oncopelti* and cyt c_{558} from *Euglena gracilis*, which contain only the covalent linkage between Cys-17 and heme (*81*). In contrast to the yeast cyt *c* mutant containing the same single covalent linkage, cyt c_{557} and cyt c_{558} exhibit well-ordered folds (*81*−*83*). Additional mutations in cyt c_{557} and cyt c_{558} have clearly compensated for the expected diminution in stability resulting from loss of a covalent bond by rigidifying the protein fold (*7*). Perhaps further stabilization of the protein fold via evolution, either natural or in the laboratory, could convert cyt c_{557} and cyt c_{558} into low-spin His−Met-coordinated proteins in the absence of covalent heme−protein linkages. It should certainly be possible to further engineer the structure of heme peptide **2** to permit formation of a more realistic cyt *c* model by enhancing the strength of His coordination. Studies aimed at exploring this possibility, and for achieving a better understanding of the structural determinants for low-spin His−Met coordination in heme proteins, are in progress.

NOTE ADDED AFTER ASAP POSTING

This paper was inadvertently published 01/21/04 with refs 48−82 incorrectly numbered. The correct version was published 01/26/04.

ACKNOWLEDGMENT

The authors thank Matthew Zart for assistance in obtaining the EPR spectra.

SUPPORTING INFORMATION AVAILABLE

Data from pH titrations and ligand binding titrations. This material is available free of charge via the Internet at http://pubs.acs.org.

REFERENCES

1. Moore, G. R., and Pettigrew, G. W. (1990) *Cytochromes c. Evolutionary, Structural and Physicochemical Aspects*, Springer-Verlag, Berlin.
2. Schejter, A. (1996) in *Cytochrome c: A Multidisciplinary Approach* (Scott, R. A., and Mauk, A. G., Eds.) Chapter 8, University Science Books, Sausalito, CA.
3. Stellwagen, E., Rysavy, R., and Babul, G. (1972) *J. Biol. Chem. 247*, 8074−8077.
4. Fisher, W. R., Taniuchi, H., and Anfinsen, C. B. (1973) *J. Biol. Chem. 248*, 3188−3195.
5. Dumont, M. E., Corin, A. F., and Campbell, G. A. (1994) *Biochemistry 33*, 7368−7378.
6. Goldberg, M. E., Schaeffer, F., Guillou, Y., and Djavadi-Ohaniance, L. (1999) *J. Biol. Chem. 274*, 16052−16061.
7. Rosell, F. I., and Mauk, A. G. (2002) *Biochemistry 41*, 7811−7818.
8. Kang, X., and Carey, J. (1999) *Biochemistry 38*, 15944−15951.
9. Harbury, H. A., and Loach, P. A. (1960) *J. Biol. Chem. 235*, 3646−3653.
10. Yang, E. K., and Sauer, K. (1982) in *Electron Transport and Oxygen Utilization* (Ho, C., Ed.) p 82, Elsevier, Amsterdam.
11. Wang, J.-S., and VanWart, H. E. (1989) *J. Phys. Chem. 93*, 7925−7931.
12. Munro, O. Q., and Marques, H. M. (1996) *Inorg. Chem. 35*, 3752−3767.
13. Low, D. W., Winkler, J. R., and Gray, H. B. (1996) *J. Am. Chem. Soc. 118*, 117−120.
14. Adams, P. A. (1990) in *Peroxidases in Chemistry and Biology* (Everse, J., and Grisham, M. B., Eds.) Chapter 7, CRC Press, Boca Raton, FL.
15. Baldwin, D. A., Marques, H. M., and Pratt, J. M. (1986) *J. Inorg. Biochem. 27*, 245−254.
16. Othman, S., Le Lirzin, A., and Desbois, A. (1994) *Biochemistry 33*, 15437−15448.
17. Tezcan, F. A., Winkler, J. R., and Gray, H. B. (1998) *J. Am. Chem. Soc. 120*, 13383−13388.
18. Dickerson, R. E., Takano, T., Eisenberg, D., Kallai, O. B., Samson, L., Cooper, A., and Margoliash, E. (1971) *J. Biol. Chem. 246*, 1511−1535.
19. Bushnell, G. W., Louie, G. V., and Brayer, G. D. (1990) *J. Mol. Biol. 214*, 585−595.
20. Low, D. W., Gray, H. B., and Duus, J. O. (1997) *J. Am. Chem. Soc. 119*, 1−5.
21. Ma, J.-G., Laberge, M., Song, X.-Z., Jentzen, W., Jia, S.-L., Zhang, J., Vanderkooi, J. M., and Shelnutt, J. A. (1998) *Biochemistry 37*, 5118−5128.
22. Melchionna, S., Barteri, M., and Ciccotti, G. (1996) *J. Phys. Chem. 100*, 19241−19250.
23. Laberge, M., Vreugdenhil, A. J., Vanderkooi, J. M., and Butler, I. S. (1998) *J. Biomol. Struct. Dyn. 15*, 1039−1050.
24. Hobbs, J. D., and Shelnutt, J. A. (1995) *J. Protein Chem. 14*, 19−25.
25. Jentzen, W., Ma, J.-G., and Shelnutt, J. A. (1998) *Biophys. J. 74*, 753−763.
26. Adams, P. A., Baldwin, D. A., and Marques, H. M. (1996) in *Cytochrome c. A Multidisciplinary Approach* (Scott, R. A., and Mauk, A. G., Eds.) Chapter 20, University Science Books, Sausalito, CA.
27. Harbury, H. A., Cronin, J. R., Fanger, M. W., Hettinger, T. P., Murphy, A. J., Myer, Y. P., and Vinogradov, S. N. (1965) *Proc. Natl. Acad. Sci. U.S.A. 54*, 1658−1664.
28. Castro, C. E. (1974) *Bioinorg. Chem. 4*, 45−65.
29. Momenteau, M., and Loock, B. (1974) *Biochim. Biophys. Acta 343*, 535−545.
30. Mashiko, T., Reed, C. A., Haller, K. J., Kastner, M. E., and Scheidt, W. R. (1981) *J. Am. Chem. Soc. 103*, 5758−5767.
31. Traylor, T. G. (1981) *Acc. Chem. Res. 14*, 102−109.
32. Morgan, B., and Dolphin, D. (1987) *Struct. Bonding 64*, 115−201.
33. Arnold, P. A., Benson, D. R., Brink, D. J., Hendrich, M. P., Jas, G. S., Kennedy, M. L., Petasis, D. T., and Wang, M. (1997) *Inorg. Chem. 36*, 5306−5315.
34. Nastri, F., Lombardi, A., D'Andrea, L. D., Sanseverino, M., Maglio, O., and Pavone, V. (1998) *Biopolymers 47*, 5−22.
35. Warme, P. K., and Hager, L. P. (1970) *Biochemistry 9*, 1606−1614.
36. Buckingham, D. A., and Rauchfuss, T. B. (1978) *J. Chem. Soc., Chem. Commun.*, 705−707.
37. Selve, C., Niedercorn, F., Nacro, M., Castro, B., and Gabriel, M. (1981) *Tetrahedron 37*, 1893−1901.
38. Matile, S., and Woggon, W.-D. (1990) *J. Chem. Soc., Chem. Commun.*, 774−776.
39. Boitrel, B., Lecas-Nawrocka, A., and Rose, E. (1992) *Tetrahedron Lett. 33*, 227−230.
40. Dokoh, T., Suzuki, N., Higuchi, T., Urano, Y., Kikuchi, K., and Nagano, T. (2000) *J. Inorg. Biochem. 82*, 127−132.
41. Benson, D. R., Hart, B. R., Zhu, X., and Doughty, M. B. (1995) *J. Am. Chem. Soc. 117*, 8502−8510.
42. Munro, O. Q., and Marques, H. M. (1996) *Inorg. Chem. 35*, 3768−3779.
43. Alden, R. G., Ondrias, M. R., and Shelnutt, J. A. (1990) *J. Am. Chem. Soc. 112*, 691−697.
44. Woody, R. W. (1985) in *The Peptides: Analysis, Synthesis, Biology* (Hruby, V. J., Ed.) Chapter 2, Academic Press, Orlando, FL.

45. Urry, D. W., and Pettegrew, J. W. (1967) *J. Am. Chem. Soc. 89*, 5276−5283.
46. Blauer, G., Sreerama, N., and Woody, R. W. (1993) *Biochemistry 32*, 6674−6679.
47. Ma, J.-G., Vanderkooi, J. M., Zhang, J., Jia, S.-L., and Shelnutt, J. A. (1999) *Biochemistry 38*, 2787−2795.
48. Deleted in proof.
49. Haddad, R. E., Gazeau, S., Pecaut, J., Marchon, J.-C., Medforth, C. J., and Shelnutt, J. A. (2003) *J. Am. Chem. Soc. 125*, 1253−1268.
50. Scheidt, W. R., and Lee, Y. J. (1987) *Struct. Bonding 64*, 1−70.
51. Wang, J.-S., Tsai, A.-L., Palmer, G., and Van Wart, H. E. (1992) *J. Biol. Chem. 267*, 15310−15318.
52. Munro, O. Q., de Wet, M., Pollak, H., van Wyk, J., and Marques, H. M. (1998) *J. Chem. Soc., Faraday Trans. 94*, 1743−1752.
53. Palmer, G. (1980) in *Iron Porphyrins* (Lever, A. B. P., and Gray, H. B., Eds.) pp 43−88, Addison-Wesley, Reading, MA.
54. Kennedy, M. L., Silchenko, S., Houndonougbo, N., Gibney, B. R., Dutton, P. L., Rodgers, K. R., and Benson, D. R. (2001) *J. Am. Chem. Soc. 123*, 4635−4636.
55. Spiro, T. G. (1987) in *Biological Applications of Raman Spectroscopy* (Spiro, T. G., Ed.) John Wiley & Sons, New York.
56. Roberts, G. P., Thorsteinsson, M. V., Kerby, R. L., Lanzilotta, W. N., and Poulos, T. L. (2001) *Prog. Nucleic Acid Res. Mol. Biol. 67*, 35−63.
57. Carrell, C. J., Schlarb, B. G., Bendall, D. S., Howe, C. J., Cramer, W. A., and Smith, J. L. (1999) *Biochemistry 38*, 9590−9599.
58. Rosell, F. I., Ferrer, J. C., and Mauk, A. G. (1998) *J. Am. Chem. Soc. 120*, 11234−11245.
59. Assfalg, M., Bertini, I., Dolfi, A., Turano, P., Mauk, A. G., Rosell, F. I., and Gray, H. B. (2003) *J. Am. Chem. Soc. 125*, 2913−2922.
60. Lushington, G. R., Cowley, A. B., Silchenko, S., Lukat-Rodgers, G. S., Rodgers, K. R., and Benson, D. R. (2003) *Inorg. Chem. 42*, 7550−7559.
61. Marques, H. M., Munro, O. Q., Munro, T., de Wet, M., and Vashi, P. R. (1999) *Inorg. Chem. 38*, 2312−2319.
62. Schejter, A., and Saludjian, P. (1967) *Biopolymers 5*, 788−790.
63. Schejter, A., Plotkin, B., and Vig, I. (1991) *FEBS Lett. 280*, 199−201.
64. Lee, K.-H., Kennedy, M. L., Buchalova, M., and Benson, D. R. (2000) *Tetrahedron 56*, 9725−9731.
65. Koshy, T. I., Luntz, T. L., Schejter, A., and Margoliash, E. (1990) *Proc. Natl. Acad. Sci. U.S.A. 87*, 8697−8701.
66. Banci, L., Rosato, A., and Turano, P. (1996) *JBIC, J. Biol. Inorg. Chem. 1*, 364−367.
67. Kolczak, U., Hauksson, J. B., Davis, N. L., Pande, U., de Ropp, J. S., Langry, K. C., Smith, K. M., and La Mar, G. N. (1999) *J. Am. Chem. Soc. 121*, 835−843.
68. Babul, J., and Stellwagen, E. (1972) *Biochemistry 11*, 1195−1200.
69. Hamada, K., Bethge, P. H., and Mathews, F. S. (1995) *J. Mol. Biol. 247*, 947−962.
70. Moore, G. R., Williams, R. J. P., Peterson, J., Thomson, A. J., and Mathews, F. S. (1985) *Biochim. Biophys. Acta 829*, 83−96.
71. Bullock, P. A., and Myer, Y. P. (1978) *Biochemistry 17*, 3084−3091.
72. Wu, J.-Z., La Mar, G. N., Yu, L. P., Lee, K.-B., Walker, F. A., Chiu, M. L., and Sligar, S. G. (1991) *Biochemistry 30*, 2156−2165.
73. Feng, Y., Sligar, S. G., and Wand, A. J. (1994) *Nat. Struct. Biol. 1*, 30−35.
74. Fuentes, E. J., and Wand, A. J. (1998) *Biochemistry 37*, 3687−3698.
75. Barker, P. D., Nerou, E. P., Freund, S. M. V., and Fearnley, I. M. (1995) *Biochemistry 34*, 15191−15203.
76. Arnesano, F., Banci, L., Bertini, I., Ciofi-Baffoni, S., Woodyear, T. d. L., Johnson, C. M., and Barker, P. D. (2000) *Biochemistry 39*, 1499−1514.
77. Gonzales, G., Dioum, E. M., Bertolucci, C. M., Tomita, T., Ikeda-Saito, M., Cheesman, M. R., Watmough, N. J., and Gilles-Gonzalez, M.-A. (2002) *Biochemistry 41*, 8414−8421.
78. Sligar, S. G., Egeberg, K. D., Sage, J. T., Morikis, D., and Champion, P. M. (1987) *J. Am. Chem. Soc. 109*, 7896−7897.
79. Rodriguez, J. C., and Rivera, M. (1998) *Biochemistry 37*, 13082−13090.
80. Falzone, C. J., Mayer, M. R., Whiteman, E. L., Moore, C. D., and Lecomte, J. T. J. (1996) *Biochemistry 35*, 6519−6526.
81. Pettigrew, G. W., Leaver, J. L., Meyer, T. E., and Ryle, A. P. (1975) *Biochem. J. 147*, 291−302.
82. Stellwagen, E., and Cass, R. (1974) *Biochem. Biophys. Res. Commun. 60*, 371−375.
83. Brems, D. N., and Stellwagen, E. (1983) *J. Biol. Chem. 258*, 10919−10923.

BI035531P